Icarus 210 (2010) 823–831

Contents lists available at ScienceDirect

Icarus

journal homepage: www.elsevier.com/locate/icarus

Characterization of Titan's Ontario Lacus region from Cassini/VIMS observations

M.L. Moriconi [a,*], J.I. Lunine [b,e], A. Adriani [b], E. D'Aversa [b], A. Negrão [b,c], G. Filacchione [d], A. Coradini [b]

[a] Institute of Atmospheric Science and Climate-CNR, Via Fosso del Cavaliere 100, I-00133 Rome, Italy
[b] IFSI–INAF, Via Fosso del Cavaliere 100, I-00133 Rome, Italy
[c] Escola Superior de Tecnologia e Gestão de Leiria, Campus 2, Morro do Lena-Alto do Vieiro, P-2411 Leiria, Portugal
[d] IASF–INAF, Via Fosso del Cavaliere 100, I-00133 Rome, Italy
[e] Department of Physics, University of Rome Tor Vergata, Via della Ricerca Scientifica 1, 00133 Roma, Italy

ARTICLE INFO

Article history:
Received 15 October 2009
Revised 22 July 2010
Accepted 27 July 2010
Available online 3 August 2010

Keywords:
Titan
Satellites, Surfaces
Infrared observations
Image processing

ABSTRACT

Liquid hydrocarbons were long predicted on Titan's surface before the RADAR instrument onboard Cassini detected lakes poleward of 70°N in July 2006. Before that the Cassini Imaging Science Subsystem (ISS) observed a lake-like feature in the South Pole, named Ontario Lacus, in July 2004. Here we analyze one observation of Ontario Lacus taken by the Visual and Infrared Mapping Spectrometer (VIMS) on 2007 December 5, during the T 38 flyby. This is the best spatially resolved image of a Titan lake to date by an imaging spectrometer, and has been previously reported in Brown et al. (Brown, R.H., Soderblom, L.A., Soderblom, J.M., Clark, R.N., Jaumann, R., Barnes, J.W., Sotin, C., Buratti, B., Baines, K.H., Nicholson, P.D. [2008]. Nature 454, 607–610) and in Barnes et al. (Barnes, J.W. et al. [2009]. Icarus 201, 217–225). The observing geometry and our data processing will be explained, followed by a discussion of the main characteristics of the image. The analyzed image covers a small portion of Ontario Lacus and shows what appears from RADAR data to be a region of modest slope ("ramp") adjacent to the dark lake itself. Our analysis of 5.0 μm spectral data suggests that the previously reported absorption feature of ethane seen at shorter wavelengths may be produced by damp sediments adjacent to the main liquid basin. The latter appears to be absorbing all of the photons incident upon it in the 5 μm spectral region and shows no discernible absorption features. A characterization of the basin composition and morphology is developed with the help of ISS and RADAR observations. The simplest model consistent with the data is an optically deep lake surrounded by a region in which ethane, propane, possibly methane, and other, less volatile hydrocarbons and nitriles are present mixed into spectroscopically neutral sediments. The dominance of relatively low vapor pressure organics outside the lake itself suggests a retreat of Ontario Lacus associated with evaporation on seasonal or longer timescales, consistent with analysis of RADAR and ISS images.

1. Introduction

Although both Imaging Science Subsystem (ISS) (Porco et al., 2005) and RADAR (Elachi et al., 2004) observations from the Cassini spacecraft detected the existence of dark surface features interpreted as liquid-filled lakes and seas, only in December 2007 did the Visual and Infrared Mapping Spectrometer (VIMS) (Brown et al., 2004) provide spectroscopic observations of one of these structures. Approximately centered at 183°W, 72°S, and named Ontario Lacus for its similarity in size and form to Lake Ontario on Earth, this is now the best-studied lake on Titan thanks to the seasonal phase of Titan which was southern summer during the primary Cassini mission from 2004 to 2008. Using specific algorithms based on the NAIF-SPICE tools (Acton, 1996) in order to accurately calculate the observational geometries, we have unambiguously determined the portions of the lake seen by VIMS in three consecutive observations of Ontario Lacus by the Cassini Orbiter. In doing so, we have accomplished a co-registration of the sequence of observations at 5.0 μm with the whole lake as imaged by the ISS narrow-angle camera (NAC) in the June 2005 encounter. Ample evidence exists that the putative lakes and seas are filled with liquid (Lunine and Lorenz, 2009). Given the thermodynamic conditions, the abundance of methane in the atmosphere, and the production of ethane as the dominant photochemical byproduct of methane, the lake composition should be dominated by methane, ethane, or both (Stofan et al., 2007), along with a second product of methane photolysis, propane, which is liquid under Titan surface conditions and highly soluble in ethane and methane (Cordier et al., 2009). Spectroscopic detection of these hydrocarbons is complicated both by the large amount of methane in the atmosphere, which effectively blacks out the portions of the

* Corresponding author. Fax: +39 0620660291.
E-mail address: m.moriconi@isac.cnr.it (M.L. Moriconi).

0019-1035/$ - see front matter © 2010 Elsevier Inc. All rights reserved.
doi:10.1016/j.icarus.2010.07.023

spectrum where we expect to see liquid methane, and by the lakes themselves, which are at least many meters deep based on the absorption properties of these materials at centimeter wavelength (Paillou et al., 2008). The optical depth in the absorption bands of both methane and ethane should be very large in the lakes unless they are polluted with a large amount of suspended debris. The weak absorption feature of ethane in the 2.0 μm atmospheric window reported by Brown et al. (2008), is difficult to understand unless the lake is extremely shallow (Clark et al., 2009). We have carried out an analysis of VIMS data in the 5.0 μm methane atmospheric spectral window and conclude that the region adjacent to the lake contains ethane, which might be responsible for the weak feature seen at shorter wavelengths. Then, we hypothesize that sediments adjacent to the lake basin itself are soaked in ethane, methane, and other less volatile hydrocarbons, exposed by progressive evaporation of the lake on seasonal or longer timescales.

2. Observations and mapping

On 2007 December 5 VIMS observed Titan's South Polar Region during the T 38 Cassini flyby. The Ontario Lacus observations were acquired during a fast spacecraft passage over Titan's South Pole, near orbital perihelion. A geometrical reconstruction of the whole sequence is shown in Fig. 1, with the aim of identifying what portion of the lake would have been seen by VIMS, where the projection of the Cassini trajectory is denoted by a green line and the terminator by a red one.

Four cubes covering the Ontario region were acquired during the flyby, but only three of them – those reported in Table 1 – in our opinion, show a spectral and spatial featuring, particularly in the CH_4 spectral window at 5 μm, suitable to carry out a satisfactory match with the ISS camera image.

The three selected VIMS cubes observe approximately the same surface region, but at increasing spacecraft distances (i.e. at decreasing spatial resolution ranging from 1.5 to 6 km for the nearest to 3.5–45 km for the farthest observation) and moving in a northwestward direction. In Table 1 some of their average characteristics are listed (mean distance, viewing angle, sub-spacecraft point position, average spatial resolution) and in Fig. 2 the sequence of VIMS observations is reported at the top.

The data have been geometrically calibrated using *ad hoc* algorithms based on NAIF-SPICE tools (Acton, 1996). In view of a spectral analysis, connected to the removal of the atmosphere by means of radiative transfer calculations, we radiometrically calibrated the images in spectral radiance ($W/m^2/nm/ster$) using the RC17 calibration pipeline (McCord et al., 2004; Filacchione, 2006; Filacchione et al., 2007).

The georeferencing allows the bright region in the upper right corner of the third cube to be interpreted as the southeast limb of Titan, consistent with the spacecraft's direction of motion and the instrumental line of sight, as shown in Fig. 1. This feature allowed us to correctly position the VIMS images and match them with the ISS one.

Image processing techniques have been applied to the 5.0 μm sequence at the top of Fig. 2 in order to simplify the successive mapping procedures. In the image processing procedures applied here we did not perform any averaging among the VIMS spectral channels to maintain the possibility of getting some information about the composition of different regions by analyzing the spectral shape in the observed wavelength range. A destriping algorithm, specifically developed for VIMS (Adriani et al., 2007), has been applied to the three cubes, followed by a low-pass filtering based on Gauss kernel (van den Boomgaard and van der Weij, 2001). The result of this processing is reported at the bottom of Fig. 2.

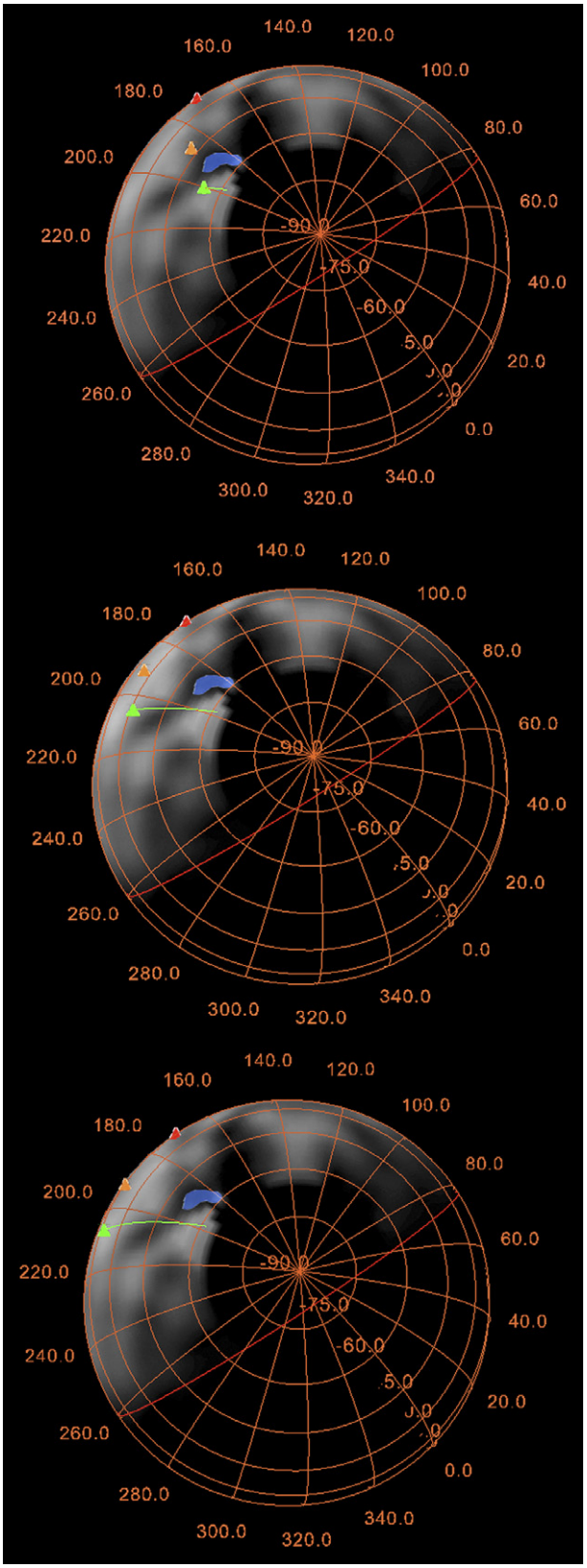

Fig. 1. Geometrical reconstruction of the sequence of Cassini/VIMS observations of Ontario Lacus on Titan, during the T 38 flyby. In the pictures the triangles indicate the sub-spacecraft point (green), the sub-solar point (red) and the sub-reflection point (orange). The projection of the Cassini trajectory is denoted by the green line and the terminator by the red one. A sketch of Ontario Lacus is also given to clarify the sequence of observations. The reported sequence starts at 00:11:31.644 and finishes at 00:31:25.673. The three pictures, from the top to the bottom, represent the simulations of the V1575506843, V1575507241 and V1575507639 cubes respectively.

Table 1
VIMS observations analyzed.

Cube name	Average distance (km)	Average viewing angle (°)	Sub-spacecraft lat./lon.	Average spatial resolution (km)
V1575506843_1.QUB	3500	65	−42.27/156.69E	4.0
V1575507241_1.QUB	6000	74	−24.84/153.82E	11.5
V1575507639_1.QUB	8500	78	−15.14/152.52E	20.0

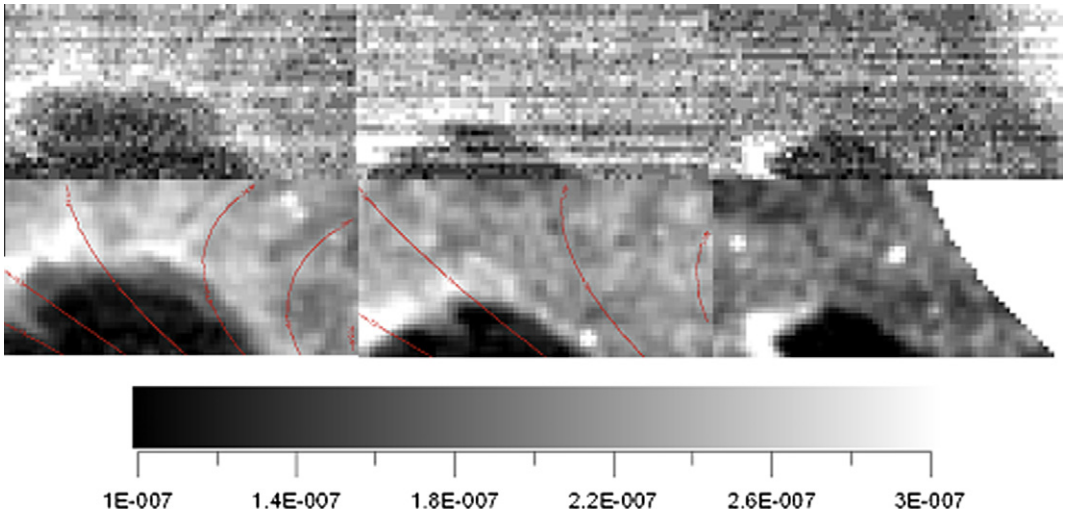

Fig. 2. The sequence of the original 5 μm VIMS images of Ontario Lacus from the cubes V1575506843, V1575507241 and V1575507639 is reported at the top of the picture in spectral radiance units (W/m^2/nm/ster). The same sequence after the image processing is reported at the bottom. In the processed sequence the data in the last panel have been masked excluding the off-limb portion of the image. The motion distortion effect is revealed by the latitudinal grid (red lines) in the first two panels and from the limb concavity in the third one. Latitude values range from −73° to −75.5° in the left and from −72° to −76° in the central panel.

A limb distortion can be noted in the third panel at the bottom. We interpret it as a side-effect of the long exposure time used to improve the signal-to-noise ratio. As a consequence, the image footprint on the surface changes substantially during the time interval needed for the full image acquisition, producing the observed distortion. A radial component can be seen, suggesting a rotational component around the z axis in the spacecraft motion. This effect can be detected as well in the other two cubes by adding the geographical grid to them, as shown in the first two panels at the bottom of Fig. 2.

Similarly a mapping of the pixel radiances in any projection will produce a distortion in the shape of the lake with respect to the image seen by VIMS, as can be seen in Fig. 3.

To produce the maps of Fig. 3 the irregular gridded pixel values, obtained by the geometrical calibrations, went through a Delauney triangulation procedure (Lee and Schachter, 1980) and bilinearly interpolated to a regular grid.

Among the material publicly accessible on the Cassini/ISS website (http://ciclops.org/ir_index_main/Cassini), a particular image, showing Ontario Lacus imaged by the NAC during the sequence

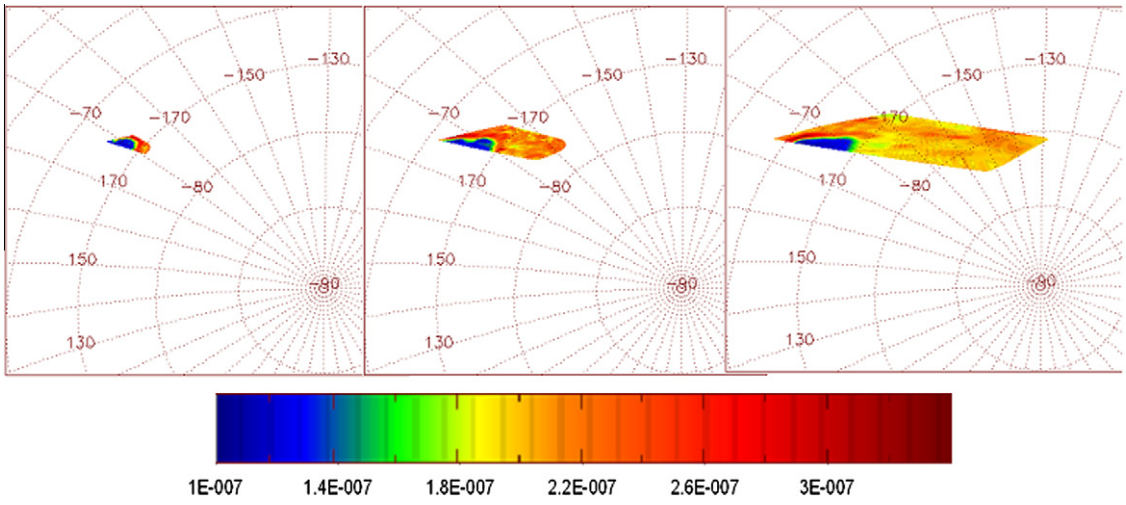

Fig. 3. The 5 μm VIMS images V1575506843, V1575507241 and V1575507639 in satellite projection. This projection has been selected to reproduce that of ISS narrow-angle camera at the time of its first observation (June 2005) of the Ontario region. The mapped values are in the same units of the original sequence reported in Fig. 2, W/m^2/nm/ster.

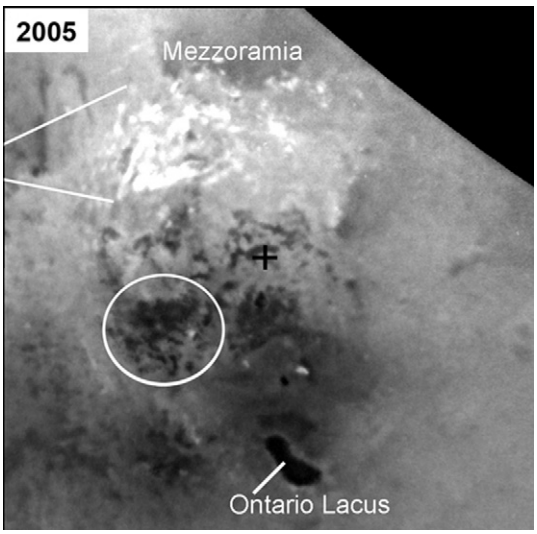

Fig. 4. The June 6, 2005 observation of the ISS narrow-angle camera of the Titan's South Pole region: besides Ontario Lacus, the South Pole (black cross), the dark area Mezzoramia, some other lake features (white circled) and some probable clouds (white lines) are indicated (PIA 11147, Credit: NASA/JPL/Space Science Institute).

ISS_009TI_COMPMAP002_CIRS the June 6 2005, has been selected for comparison with VIMS (Fig. 4), because of its well detailed and contrasted appearance.

The ISS-NAC original data on the PDS website for this image consisted of a sequence of similar observations, already containing suitable kernels information for a correct georeferenciation by means of the NAIF-SPICE tool. These observations are characterized by the use of a variety of filters combination. We selected for our co-registration the N1496745450_1.IMG image, filtered by an IR polarizer in conjunction with a narrowband, centered at 938 nm, that assured a better penetration through the Titan haze and viewing of surface spatial features with respect to other combinations. Then we co-registered and overlapped the VIMS and ISS-NAC data by means of the correspondence of their geographical coordinates. The same satellite projection has been selected to map both the VIMS pixel radiances and the ISS-NAC pixel units, assuming a vertical perspective of the satellite position, centered at 85°S and 180°W, and a distance from Titan similar to that of V1575506843 VIMS observation. In Fig. 5 the ISS mapped observation is reported both without (panel a) and with (panels b, c and d) overlaying color maps of the VIMS radiances at 5 μm.

Looking particularly at the 5b, 5c and 5d panels the blue region stands for the lowest radiance value in the adopted color table, consistent with a sink for the photons. This visualization seems to indicate that the Ontario southern border had moved partially inward (toward the lake center) with respect to the shoreline of the shape imaged by ISS at 938 nm. A progressive loss of shape and color definition can be noticed passing from panels (b) to (d). This effect can be ascribed to the growing pixel deformation, due to the corresponding increase of the viewing angle.

3. Interpretation and spectral analysis

VIMS can observe Titan's surface through the methane spectral windows at 2.0, 2.8 and 5.0 μm. For wavelengths <2.0 μm the thick atmospheric layer of organic aerosols extinguishes most of the solar radiation before it can reach the surface in and out of the methane windows. In the spectral windows between 0.9 and 2.0 μm the surface can be distinguished at very small viewing angles, but multiple scattering, particularly at high air masses, hides most of the details in the 2.0 and 2.8 μm windows. Thus in the observations we have analyzed, characterized by low viewing angles and grazing incidence of solar radiation, the surface features are truly well defined only in the 5.0 μm spectral window. Motivated in part by RADAR altimeter observations (Lorenz et al., 2009) showing a modest slope in the ramp adjacent to the western side of Ontario Lacus, which then steepens further to the west, we hypothesize that there are three distinct physiographic regions from the 5.0 μm spatial frame in the first panel of Fig. 2:

1. A liquid reservoir (the darker area in the image) where the solar radiation is essentially fully extinguished along a physical distance through the liquid small compared to the lake depth.
2. A relatively uniform area, perhaps sedimentary deposits or exposed lakebed, seen as the dark gray region surrounding the reservoir. We call this the "ramp", based on RADAR altimetry.
3. An irregular ridge, suggesting non-uniform elevation, morphology, or both, seen as the brighter area in the image.

Discrimination among the regions has been also made on a radiance basis, co-adding the 13 channels in the 5 μm methane window (from 4.87 μm to 5.07 μm) and using it for a spectral average. From this result three regions representative of the physiographic areas have been selected on the base of their radiance values:

- Lake bed $\leqslant 1 \cdot e{-}07$ W/m^2/nm/ster,
- $1 \cdot e{-}07 <$ ramp $\leqslant 2 \cdot e{-}07$ W/m^2/nm/ster,
- $2 \cdot e{-}07 <$ ridge W/m^2/nm/ster.

Not all the pixels meeting these conditions have been selected; rather only a visual selection representative of the regions chosen for the analysis has been made.

These three regions are reported in red, cyan and green respectively in Fig. 6.

The hypothesis, then, is that Ontario Lacus is a basin with an optically deep liquid surrounded by an area of sediments, soaked with ethane and other organics. Because of its long pathlength, we assume that the spectra acquired of the lake basin itself are only due to the atmosphere contribution (both scattering and fluorescent sources), motivated also from the calculations reported in Brown et al. (2008), explained in the caption of Fig. 3. In other words, the lake area will be considered a sink for the radiation at 5.0 μm. The latter hypothesis is consistent with other VIMS observations – to which we do not refer explicitly here – viewing the limb of Titan (see e.g. Baines et al., 2006). In Fig. 7, the radiance spectra, averaged over the regions of interest, are compared with a VIMS limb spectrum at 60 km tangent altitude, namely the distance from the surface of the line of sight (LOS) relative to the observed pixel, and 75°S, with the Sun behind the observer. It can be seen that the spectral shapes in nadir viewing appear very similar to the case of limb-viewing geometry shortward of 4.87 μm (channel 241 of VIMS-IR).

The generally lower intensity in the nadir viewing spectra can be attributed to the different radiation pathways in the two geometries, the radiance in the nadir case experiencing a bigger extinction along the path to and from the surface. At wavelengths greater than 4.87 μm the nadir spectra split, depending on the different scattering properties of the surfaces the radiation encounters. In order to remove the atmospheric contribution, a simple algorithm, developed for AVIRIS data validation (Miesch et al., 2005) has been applied to remove the atmosphere contribution from the ramp and ridge spectra. The analytical formulation of this algorithm provides a useful heuristic understanding of how the various parameters enter into the analysis:

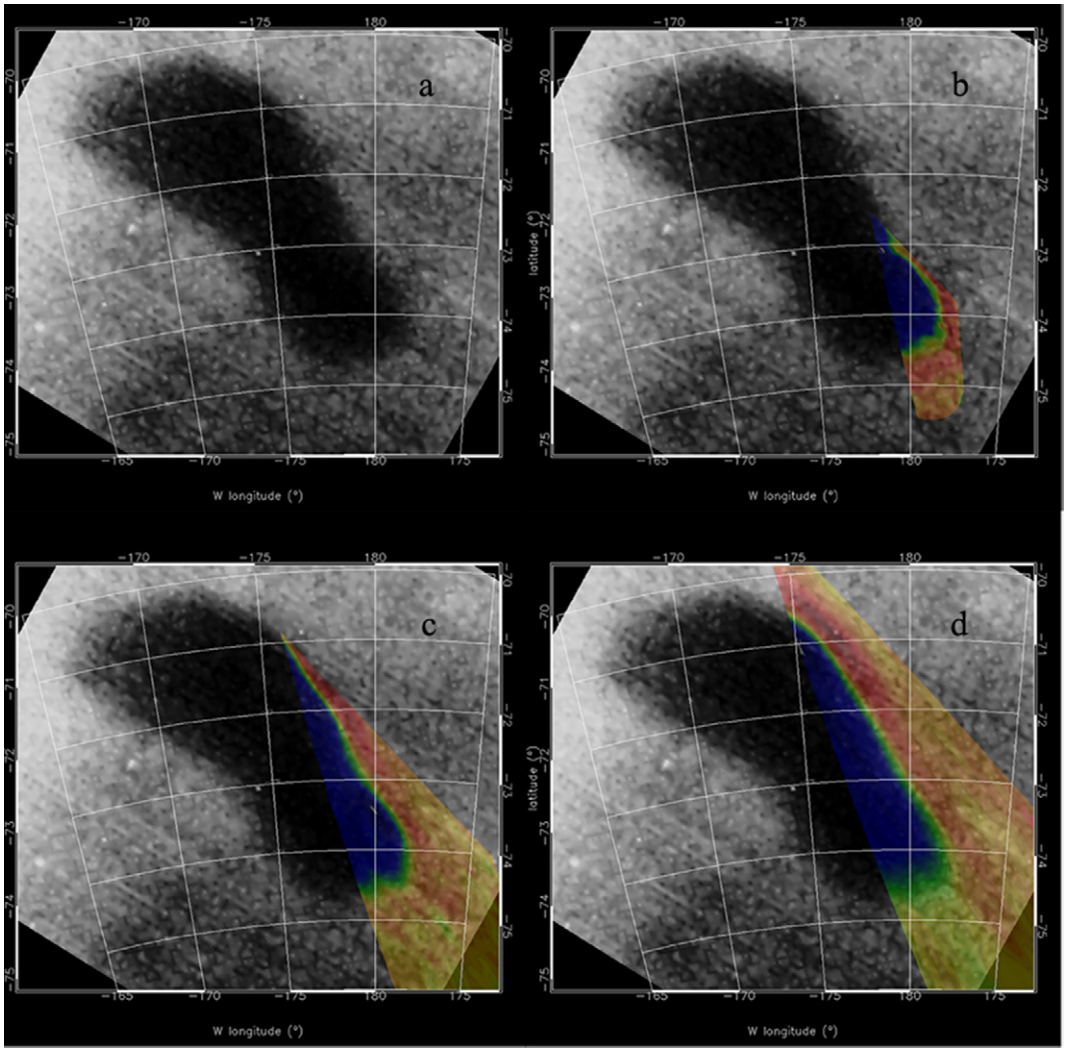

Fig. 5. Overlapping of the three cube maps of Fig. 3 on the 2005 ISS N1496745450_1.IMG observation is reported in the (b), (c) and (d) panels of this figure. In panel (a) the same satellite projection used for VIMS maps of Fig. 3 has been applied to the ISS observation. The colorbar is the same applied for Fig. 3.

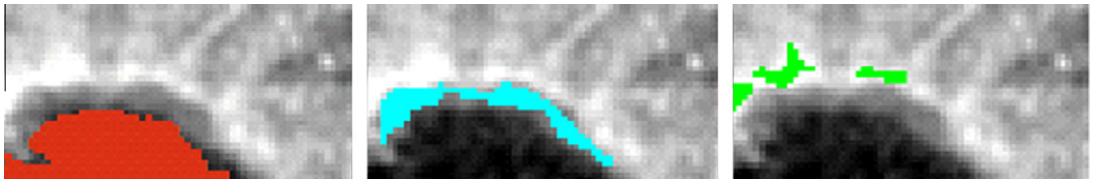

Fig. 6. In the three panels the main morphological characteristics identified for the Ontario's area are filled in red (liquid reservoir, 368 pixels), cyan (ramp, 134 pixels) and green (ridge, 63 pixels). An average spectral behavior has been calculated for each of these characteristic regions. The same color indexing of Fig. 2 has been used.

$$L_S = L_A + T \times cos(\theta) \times L_0$$

where L_S is the radiance at sensor, L_A is the atmospheric contribution (scattering and emissions), T is the atmospheric transmission at nadir, θ is the viewing angle and L_0 is the radiance scattered by the surface in the Lambertian approximation. Under the hypothesis of $L_0 = 0$ (the lake as a sink of photons), $L_S \equiv L_A$. Here we limit our analysis to between about 3.3 and 5.1 μm, since in this spectral range the main contribution comes from atmospheric emissions (local thermal equilibrium or nonlocal thermal equilibrium) rather than to the atmospheric scattering, as can be seen from Fig. 7. Here the CH_4, the CH_3D and the CO contributions can be recognized in the plotted spectral behaviors. Because the analyzed region is limited both in geographical extension and in viewing angles, we can assume that the atmospheric contribution evaluated on the lake area should also be the same for the regions where $L_0 \neq 0$. Therefore the average lake spectrum (or in other words the atmosphere contribution, as the lake has been considered to absorb all the radiation that reaches it) has been subtracted from the ramp- and ridge-average spectral radiances, simulating the removal of atmosphere scattering and emission. This operation enhanced some spectral features in the remaining surface spectra, reducing the rest of the spectral range to white noise (Fig. 8).

In order to make some hypotheses about candidate materials that could be responsible for the spectral signatures, we have considered a list of alkanes and nitriles taken from the paper recently

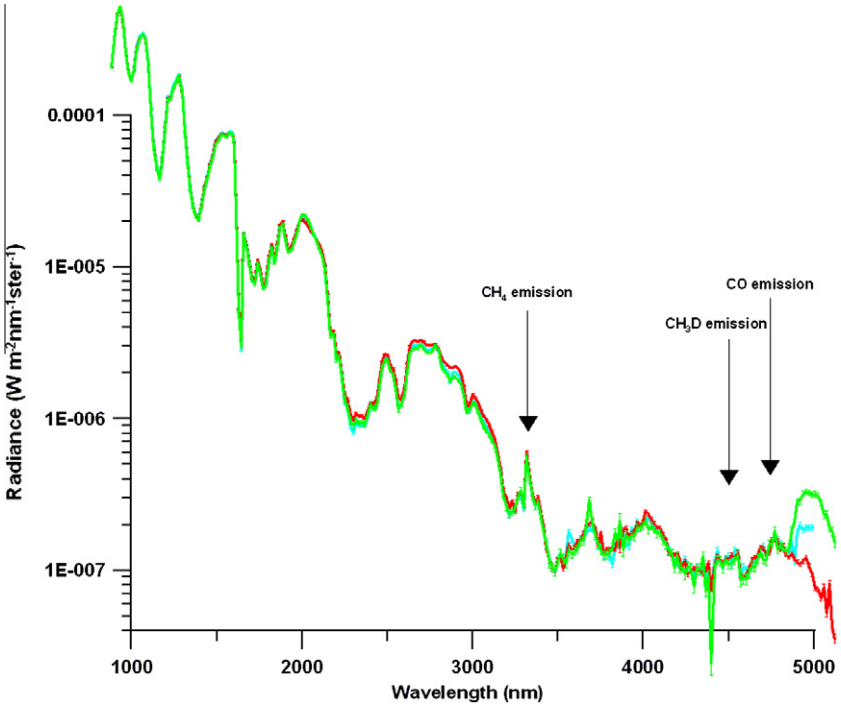

Fig. 7. The average spectral behaviors for the lake's (red), ramp's (cyan) and ridge's (green) areas are compared with a single pixel spectrum in limb geometry (black) at the same latitude and with the Sun behind the observer (S32-GLOBMAP002-V1563525149). The atmospheric emissions for methane, deuterated methane and carbon monoxide are also indicated. Note that the *y*-axis is logarithmic in order to enhance details in the long wavelengths range.

published by Clark et al. (2009). On the basis of evidence elsewhere on Titan (Lunine and Lorenz, 2009), thermodynamic considerations (Cordier et al., 2009) and laboratory measurements (Clark et al., 2009), the two alkanes methane (CH_4) and ethane (C_2H_6) are the most probable candidate, in unconstrained mixing ratio, for the liquid in the basin portion of Ontario Lacus. Nitrogen should be present in small amounts as well but spectroscopically is difficult to see (the pressure-induced fundamental at 4.3 μm is buried in atmospheric methane absorption). Propane (C_3H_8), acetylene (C_2H_2), butane (C_4H_{10}) and hydrogen cyanide (HCN) possess features (Clark et al., 2009) that are in general agreement with the ridge spectrum of the region. Benzene (C_6H_6), as it has been already observed elsewhere on Titan (Clark et al., 2009) was considered as a possible constituent. However it does not appear to be present, based on the analysis we now describe. The Spectral Angle Mapper (SAM) is a physically-based spectral classification that uses a *n*-D angle to match pixels to reference spectra, where *n* is the number of selected bands and D is a shorten form for dimension (Kruse et al.,

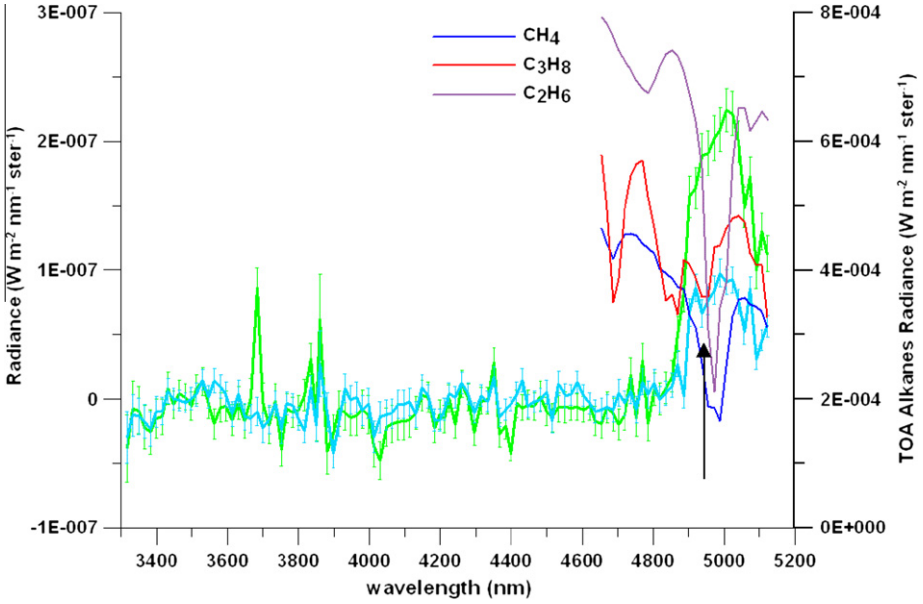

Fig. 8. The average spectral behaviors for the ramp's (cyan) and ridge's (green) areas after the subtraction of the lake contribution. The methane (blue), propane (red) and ethane (maroon) spectral behaviors at the top of atmosphere (TOA) are reported in radiance ($W/m^2/nm/ster$), with reference to the *y*-axis at right of the plot, for comparison. A spectral signature at 4.94 μm (black arrow) could indicate a different composition between the ramp and the ridge surface albedo.

Table 2
Target detection summary. The bands range from 241 to 253 (4.87–5.07 μm). Six target spectra were selected (listed under target name in the table). A forward MNF transform (3 bands) was run. The Spectral Angle Mapper (SAM) was used.

Rule threshold table			
Target name	Method	Rule threshold	Revealed
C_2H_6	SAM	0.150	Yes
C_3H_8	SAM	0.150	Yes
CH_4	SAM	0.150	Yes
C_2H_2	SAM	0.150	Yes
C_4H_{10}	SAM	0.150	Yes
C_6H_6	SAM	0.150	No
HCN	SAM	0.150	Yes

1993; Kruse, 2007). SAM compares the angle between the end member spectrum vector and each pixel vector in *n*-D space. Smaller angles represent closer matches to the reference spectrum and higher probability of being a target. The maximum angle threshold for a SAM analysis can be specified. Decreasing the threshold usually results in fewer matching pixels (better matches to the reference spectrum). Increasing the threshold may result in a more spatially coherent image; however, the overall pixel matches will not be as good as for the lower threshold. In the present analysis a quite conservative threshold of 0.15 radians has been applied, as reported in Table 2 together with a summary of the operations carried out in our SAM analysis. The results of this target detection algorithm application are reported in Fig. 9.

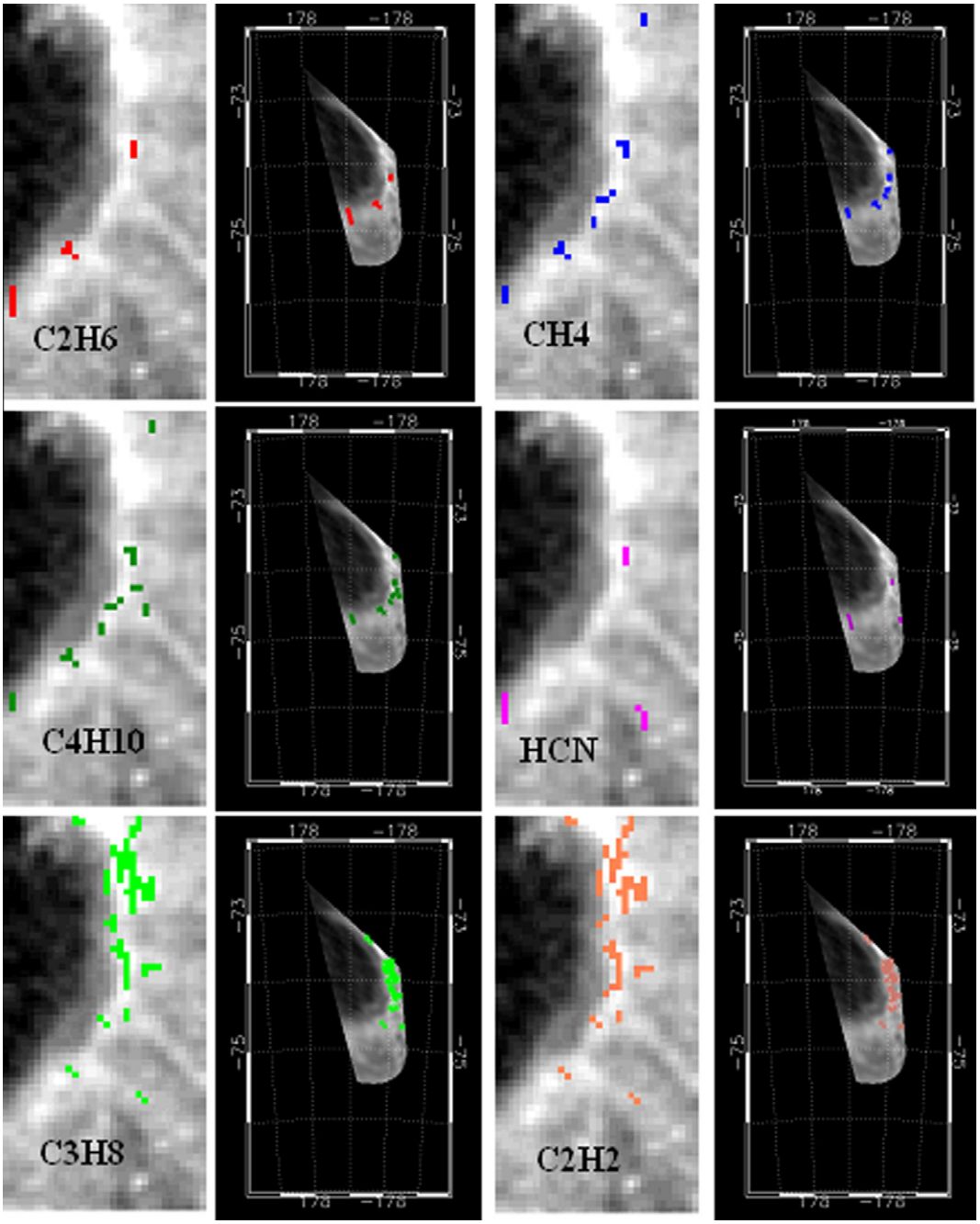

Fig. 9. Tentative surface composition of the Ontario's region based on SAM spectral classification algorithm. From the left to the right and from the top to bottom C_2H_6, CH_4, C_4H_{10}, HCN, C_3H_8, C_2H_2 are reported. C_6H_6 resulted not classified. The target detection result has been placed on the processed VIMS image to highlight the prevailing concentrations of each single end member. At the right of each image a mapped version in satellite projection has been added.

These analyses have been applied to the original image without any image processing (Fig. 2) in order to avoid any possible spectral contamination among adjacent pixels. The SAM classification would seem to suggest that ethane and methane (possibly with butane and/or hydrogen cyanide) can be recognized in what we interpret as the "retreated lakebed", namely the region that in the analyzed VIMS image fills the right portion of the frame.

4. Discussion and conclusions

In the "ramp" region adjacent to the lake propane, butane, and acetylene seems to predominate. This result is consistent with the hypothesis that propane is dissolved in the lake as a significant component along with ethane and methane (Cordier et al., 2009). Butane and acetylene dissolve in the lake liquid as well, but could also be present in the bottom sediments. As the lake shrunk over the southern summer, these components may have become exposed by the retreating liquid, or precipitated out, or both. All three have similar volatilities (Fig. 10). However, it remains to be explained why the much more volatile methane and ethane are present over a portion of the lake boundary as well.

Both may be seeping into the surrounding soil from the lake itself, but methane in particular might also be recharged by springtime precipitation (Turtle et al., 2009). This is supported by its greater abundance in the ramp region than that of ethane. The absence or very sparse presence of any of these constituents far from the lake reinforces our view that we are seeing material whose deposition is related to the immediate lake environment, or in fact the retreat of the lake itself. Hydrogen cyanide appears to be present in only three locations in the VIMS image, one of which is so close to the edge of the image that its presence there (as well as that of other species in those same pixels) could be an artifact. One photochemical model (Lavvas et al., 2008) predicts its net stratospheric production rate to be comparable to that of acetylene – the two being the most abundant products of the photochemistry which are solid at Titan's surface. Other models (e.g., Wilson and Atreya, 2004) predict lesser production rates of HCN relative to acetylene. Its relative scarcity might also be due to, or exacerbated by, its much lower volatility than the other identified components (Fig. 10). The absence of benzene, which is a product of the (exothermic) cyclization of acetylene and is seen by VIMS elsewhere on Titan (Clark et al., 2010), argues that the acetylene seen in the data has been exposed or come out of solution from the lake relatively recently – again consistent with a scenario in which the lake is currently shrinking. Elsewhere on Titan, where lakes are not present, acetylene has had plenty of time to be exposed to the low cosmic ray flux which might induce it to convert into benzene (Zhou et al., 2010).

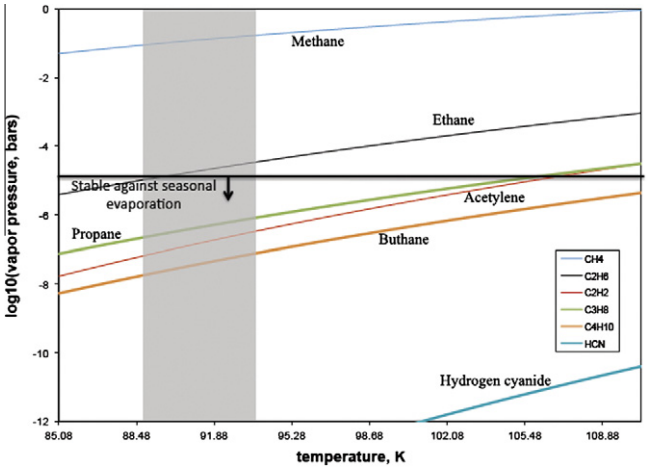

Fig. 10. Vapor pressure versus surface temperature of potential constituents around the Ontario Lacus basin. The gray bar indicates plausible temperatures of the lakes from models (Tokano, 2009). The black horizontal line divides components according to their volatility: below the line, vapor pressures are too low to permit significant evaporation of the liquid over a Titan year, regardless of the availability of solar energy. For relevant temperatures at Ontario Lacus, only methane contributes to a reduction in lake level; propane and the other constituents are left behind. Ethane is a marginal case; some evaporation of ethane does occur seasonally, but its behavior is more like propane than like methane. Vapor pressures from Brown and Ziegler (1980), Perry and Porter (1926), and the NIST Chemistry Webbook http://webbook.nist.gov/chemistry/.

The terrestrial analogy to Ontario Lacus might be that of a salty lake which is retreating, thereby exposing sand dampened by water and coated with salts along its periphery. In the Titan case the methane substitutes for water and compounds like acetylene function as the salt. The analogy is made imperfect by the interesting complication that multiple liquid hydrocarbons of widely varying volatility appear to make up the bulk composition of Ontario Lacus on Titan. The alkane reflectances reported by Clark et al. (2010) refer to a two-way transmission of a very thin liquid film of methane and ethane, with effective pathlength of 100 μm. In a geophysical scenario in which Ontario Lacus is a basin full of liquid hydrocarbons some meters or tens of meters deep, as inferred by the Cassini/RADAR tracking (Lorenz et al., 2008), the solar radiation at 5 μm would be totally extinguished in the relevant wavelength bands. This is confirmed by the average VIMS spectrum of the lake's region which does not show obvious absorption features of methane or ethane. However, an indirect determination, obtained by observing what are presumed to be sediments of ice or possibly refractory organics immediately adjacent to the lake, indicates the presence of ethane and propane of sufficiently low pathlength that the spectral signatures are weak.

Our result supports the conclusion of Brown et al. (2008) that Ontario Lacus contains ethane and methane, but adds to it the possibility that propane is present as predicted by thermodynamic models. Other data, from the Huygens probe, buttress the idea that Titan's sediments can hold measurable amounts of methane and other hydrocarbons. At the Huygens landing site, methane and ethane began evaporating from the surface once contact with the Huygens probe's warm mass spectrometer inlet was made (Niemann et al., 2005; Lorenz et al., 2006). Propane was not seen in the Huygens data, indicating either surface heterogeneity or a volatility effect having to do with the maximum temperature of the heated probe and the lower vapor pressure of propane relative to ethane and methane. In summary, our analysis of the VIMS data suggest that the region adjacent to Ontario Lacus is a shoreline in which ethane, propane, several other organic species, and possibly methane itself, saturate sediments as the lake undergoes its seasonal retreat. The spatial extent of this region – of orders kilometers – is consistent with the amount of summertime evaporation of Ontario Lacus seen through comparison of RADAR and ISS images taken four years apart (Lunine et al., 2009), and from analysis of VIMS data by Barnes et al. (2009).

Acknowledgments

We thank F. Tosi, by IFSI–INAF, for his comments regarding the surface classification. We thank the VIMS and ISS teams for planning and operations. This research has been supported by the Italian Space Agency (ASI), the Cassini Project (NASA), and the program "Incentivazione alla mobilita' di studiosi stranieri e italiani residenti all'estero."

References

Acton, C.H., 1996. Ancillary data services of NASA's navigation and ancillary information facility. Planet. Space Sci. 44 (1), 65–70.

Adriani, A., Moriconi, M.L., Filacchione, G., Tosi, F., Coradini, A., Brown, R.H., and the Cassini–VIMS Team, 2007. The de-striping of the VIMS-V images and the observations of HCN limb emission in the Titan atmosphere at 3 μm. Mem. Soc. Astron. Ital. Suppl. 11, 37–46.

van den Boomgaard, R., van der Weij, R., 2001. Gaussian Convolutions Numerical Approximations Based on Interpolation, Scale-Space and Morphology in Computer Vision. Springer, Berlin, Heidelberg. pp. 205–214.

Baines, K.H., Drossart, P., Lopez-Valverde, M.A., Atreya, S.K., Sotin, C., Momary, T.W., Brown, R.H., Buratti, B.J., Clark, R.N., Nicholson, P.D., 2006. On the discovery of CO nighttime emissions on Titan by Cassini/VIMS: Derived stratospheric abundances and geological implications. Planet. Space Sci. 54, 1552–1562.

Barnes, J.W. et al., 2009. Shoreline features of Titan's Ontario Lacus from Cassini/VIMS observations. Icarus 201, 217–225.

Brown Jr., G.N., Ziegler, W.T., 1980. In: Timmerhaus, K., Snyder, H.A. (Eds.), Advances in Cryogenic Engineering, vol. 25. Plenum Press, New York, pp. 662–670.

Brown, R.H. et al., 2004. The cassini visual and infrared mapping spectrometer (VIMS) investigation. Space Sci. Rev. 115, 111–168.

Brown, R.H., Soderblom, L.A., Soderblom, J.M., Clark, R.N., Jaumann, R., Barnes, J.W., Sotin, C., Buratti, B., Baines, K.H., Nicholson, P.D., 2008. The identification of liquid ethane in Titan's Ontario Lacus. Nature 454, 607–610.

Clark, R.N., Curchin, J.M., Hoefen, T.M., Swayze, G.A., 2009. Reflectance spectroscopy of organic compounds: 1. Alkanes. J. Geophys. Res. 114, E03001. doi:10.1029/2008JE003150.

Clark, R.N., and 15 colleagues, 2010. Detection and mapping of hydrocarbon deposits on Titan. J. Geophys. Res., in press, doi:10.1029/2009JE003369.

Cordier, D., Mousis, O., Lunine, J.I., Lavvas, P., Vuitton, V., 2009. An estimate of the chemical composition of Titan's lakes. Astrophys. J. 707, L128–L131.

Elachi, C., and 21 colleagues, 2004. RADAR: The Cassini Titan RADAR mapper. Space Sci. Rev. 115, 71–110.

Filacchione, G., 2006. Calibrazioni a terra e prestazioni in volo di spettrometri ad immagine nel visibile e nel vicino infrarosso per l'esplorazione planetaria (On ground Calibrations and in Flight Performances of VIS-NIR Imaging Spectrometers for Planetary Exploration). PhD dissertation, Università degli studi di Napoli Federico II (in Italian). <ftp://ftp.iasfroma.inaf.it/gianrico/phd/Filacchione_PHD_2006.pdf>.

Filacchione, G., and 23 colleagues, 2007. Saturn's icy satellites investigated by Cassini–VIMS I full-disk properties: 350–5100 nm reflectance spectra and phase curves. Icarus 186, 259–290.

Kruse, F.A., Lefkoff, A.B., Boardman, J.B., Heidebrecht, K.B., Shapiro, A.T., Barloon, P.J., Goetz, A.F.H., 1993. The spectral image processing system (SIPS) – Interactive visualization and analysis of imaging spectrometer data. Rem. Sens. Environ. 44, 145–163 (Special issue on AVIRIS).

Kruse, F.A., 2007. Improved multispectral mapping by spectral modeling with hyperspectral signatures. In: Proceedings, SPIE Symposium on Defense & Security, 9–13 April 2007, Orlando, FL, SPIE, vol. 6565, doi:10.1117/12.719002.

Lavvas, P.P., Coustenis, A., Vardavas, I.M., 2008. Coupling photochemistry with haze formation in Titan's atmosphere. Part II: Results and validation with Cassini/Huygens data. Planet. Space Sci. 56, 67–99.

Lee, D.T., Schachter, B.J., 1980. Two algorithms for constructing a delaunay triangulation. Int. J. Comp. Infor. Sci. 9, 219–242.

Lorenz, R.D., Niemann, H.B., Harpold, D.N., Way, S.H., Zarnecki, J.C., 2006. Titan's damp ground: constraints on Titan surface thermal properties from the temperature evolution of the Huygens GCMS inlet. Meteoritics Planet. Sci. 41, 1705–1714.

Lorenz, R.D., and 15 colleagues, 2008. Titan's inventory of organic surface materials. Geophys. Res. Lett. 35, L02206. doi:10.1029/2007GL032118.

Lorenz, R.D., 14 colleagues, and the Cassini RADAR Team, 2009. Ontario Lacus: Brilliant observations of a Titan Lake by the Cassini RADAR altimeter. Lunar Planet. Sci. XL.

Lunine, J.I., Hayes, A.G., Aharonson, O., Mitri, G., Lorenz, R., Stofan, E., Wall, S., Elachi, C., and the Cassini RADAR Team, 2009. Evidence for liquid in Ontario Lacus (Titan) from Cassini-observed changes. Bull. Am. Astron. Soc. Abstract 21.04.

Lunine, J.I., Lorenz, R.D., 2009. Rivers, lakes, dunes, and rain: Crustal processes in Titan's methane cycle. Annu. Rev. Earth Planet. Sci. 37, 299–320.

McCord, T.B., and 24 colleagues, 2004. Cassini VIMS observations of the Galilean satellites including the VIMS calibration procedure. Icarus 172, 104–126.

Miesch, C., Poutier, L., Achard, V., Briottet, X., Lenot, X., Boucher, Y., 2005. Direct and inverse radiative transfer solutions for visible and near-infrared hyperspectral imagery. IEEE Trans. Geosci. Rem. Sens. 43, 1552–1562.

Niemann, H., and 17 colleagues, 2005. The composition of Titan's atmosphere from the GCMS on the Huygens probe, and implications for the origin of nitrogen and methane. Nature 438, 779–784.

Paillou, P., Mitchell, K., Wall, S., Ruffie, G., Wood, C., Lorenz, R., Stofan, E., Lunine, J., Lopes, R., Encrenaz, P., 2008. Microwave dielectric constant of liquid hydrocarbons: Application to the depth estimation of Titan's lakes. Geophys. Res. Lett. 35, L05202. doi:10.1029/2007GL032515.

Perry, J.H., Porter, F., 1926. The vapor pressures of solid and liquid hydrogen cyanide. J. Am. Chem. Soc. 48, 299–302.

Porco, C.C., and 35 colleagues, 2005. Imaging of Titan from the Cassini spacecraft. Nature 434, 159–168.

Stofan, E.R., and 37 colleagues, 2007. The lakes of Titan. Nature 445, 61–64.

Tokano, T., 2009. Limnological structure of Titan's hydrocarbon lakes and its astrobiological implication. Astrobiology 9, 147–164.

Turtle, E.P., Perry, J.E., McEwen, A.S., Del Genio, A.D., Barbara, J., West, R.A., Dawson, D.D., Porco, C.C., 2009. Cassini imaging of Titan's high latitude lakes, clouds and south polar surface changes. Geophys. Res. Lett. 36, L02204. doi:10.1029/2008GL036186.

Wilson, E.H., Atreya, S.K., 2004. Current state of modeling the photochemistry of Titan's mutually dependent atmosphere and ionosphere. J. Geophys. Res. 109, E06002. doi:10.1029/2003JE002181.

Zhou, L., Zheng, W., Kaiser, R.I., Landera, A., Mebel, A.L., Liang, M.-C., Yumg, Y.L., 2010. Cosmic-ray-mediated formation of benzene on the surface of Saturn's moon Titan. Astrophys. J. 718, in press, doi:10.1088/0004-637X/718/2/1243.